JCB Journal of Cell Biology

REPORT

TORC1 inactivation stimulates autophagy of nucleoporin and nuclear pore complexes

Yui Tomioka[1], Tetsuya Kotani[1], Hiromi Kirisako[1], Yu Oikawa[2], Yayoi Kimura[3], Hisashi Hirano[3], Yoshinori Ohsumi[2], and Hitoshi Nakatogawa[1]

The mechanisms underlying turnover of the nuclear pore complex (NPC) and the component nucleoporins (Nups) are still poorly understood. In this study, we found that the budding yeast *Saccharomyces cerevisiae* triggers NPC degradation by autophagy upon the inactivation of Tor kinase complex 1. This degradation largely depends on the selective autophagy-specific factor Atg11 and the autophagy receptor–binding ability of Atg8, suggesting that the NPC is degraded via receptor-dependent selective autophagy. Immunoelectron microscopy revealed that NPCs embedded in nuclear envelope–derived double-membrane vesicles are sequestered within autophagosomes. At least two pathways are involved in NPC degradation: Atg39-dependent nucleophagy (selective autophagy of the nucleus) and a pathway involving an unknown receptor. In addition, we found the interaction between Nup159 and Atg8 via the Atg8-family interacting motif is important for degradation of this nucleoporin not assembled into the NPC. Thus, this study provides the first evidence for autophagic degradation of the NPC and Nups, which we term "NPC-phagy" and "nucleoporinophagy."

Introduction

Macroautophagy (hereafter autophagy) is an intracellular degradation pathway found in most eukaryotes in which different cellular components are sequestered within double-membrane vesicles called autophagosomes and transported to lytic compartments (lysosomes or vacuoles; Yang and Klionsky, 2010; Ohsumi, 2014). Although autophagic sequestration used to be deemed a nonselective process, an increasing number of studies have revealed that a wide variety of proteins and organelles are sequestered into autophagosomes in a selective manner (Kirkin, 2020; Gatica et al., 2018). In selective autophagy, proteins called autophagy receptors recognize specific cargo molecules or structures. In *Saccharomyces cerevisiae*, autophagy receptors interact with Atg11 to recruit the core Atg proteins, which initiate autophagosome formation on the cargos (Zientara-Rytter and Subramani, 2019). The receptors also bind to Atg8 on forming autophagosome membranes (isolation membranes or phagophores), thereby promoting cargo sequestration into autophagosomes (Noda et al., 2010; Johansen and Lamark, 2020).

The nuclear pore complex (NPC) is a huge protein assemblage embedded in the nuclear envelope and has vital roles in gene expression by mediating transport between the nucleus and cytoplasm as well as regulating genome architecture (Strambio-De-Castillia et al., 2010). The NPC is composed of seven substructures (the transmembrane ring, outer ring, inner ring, linker, pore filaments, nuclear basket, and cytoplasmic filaments), which are assembled by ∼30 different nucleoporins (Nups; Aitchison and Rout, 2012; Strambio-De-Castillia et al., 2010; Kim et al., 2018). As with other cellular components, to control the copy number, function, and quality of the NPC, appropriate degradation and turnover of the NPC or Nups must be important. Previous studies have revealed that the turnover rate differs substantially among Nups (Tran and Wente, 2006). In addition, a surveillance system for NPC assembly, involving the endosomal sorting complexes required for transport (ESCRT) machinery, has been reported (Webster et al., 2014). However, the cellular system that degrades the NPC or Nups is still largely unknown.

Here, we report that the NPC and Nups are selectively degraded by autophagy when Tor kinase complex 1 (TORC1) is inhibited in *S. cerevisiae*. While the whole NPC is targeted to two receptor-mediated selective autophagy pathways, unassembled Nup159, a component of the cytoplasmic filament of the NPC, is degraded by autophagy via its direct binding to Atg8.

Results and discussion

The NPC is degraded by selective autophagy under TORC1-inactivating conditions

We investigated whether the NPC is degraded by autophagy using a GFP processing assay. In this assay, autophagic degradation of

[1]School of Life Science and Technology, Tokyo Institute of Technology, Yokohama, Japan; [2]Institute of Innovative Research, Tokyo Institute of Technology, Yokohama, Japan; [3]Advanced Medical Research Center, Yokohama City University, Yokohama, Japan.

Correspondence to Hitoshi Nakatogawa: hnakatogawa@bio.titech.ac.jp.

GFP-fused proteins is assessed by monitoring the generation of GFP fragments, which are relatively resistant to vacuolar proteases. We chose a Nup from each of the seven substructures of the NPC (Fig. 1 A; Strambio-De-Castillia et al., 2010) based on the presence of human homologues and taggability and fused GFP to the C termini of these Nups. We confirmed the localization of the GFP-tagged Nups to the nuclear envelope by fluorescence microscopy (Fig. S1 A). We treated these cells with the TORC1 inhibitor rapamycin (Loewith et al., 2002; Noda and Ohsumi, 1998), which induces different types of autophagy. In immunoblotting analysis using anti-GFP antibodies, GFP fragments were detected in all cells expressing different Nups after treatment with rapamycin (Fig. 1 B). The accumulation of GFP fragments was also observed when cells were shifted to nitrogen starvation, in which TORC1 is inactivated (Fig. S1 B). GFP fragments began to appear at 8 h after rapamycin treatment (Fig. 1 C) and were not observed in *ATG1* knockout (*atg1*Δ) cells, which are defective in autophagy (Matsuura et al., 1997; Fig. 1 B and Fig. S1 B). These results suggest that Nups are degraded by autophagy when TORC1 activity is attenuated. It should be noted that in these immunoblotting experiments, the levels of GFP-tagged Nups were largely different from each other and not necessarily consistent with their previously estimated copy numbers in the NPC (Kim et al., 2018; Rajoo et al., 2018). This would be due to different efficiencies in extraction of Nups from cells and/or their transfer from SDS-PAGE gels to polyvinylidene fluoride membranes.

TORC1 inactivation induces both nonselective and selective autophagy. To determine whether autophagic degradation of Nups is selective, we examined this process in cells lacking Atg11, which, in association with autophagy receptors, plays a central role in target recognition in most selective autophagy pathways (Zientara-Rytter and Subramani, 2019). *ATG11* knockout caused marked defects in degradation of all of the GFP-tagged Nups we examined (Fig. 2 A). Autophagy receptors interact with both degradation targets and Atg8 family proteins to link the targets to forming autophagosomal membranes (Gatica et al., 2018; Kirkin, 2020). These receptors contain the Atg8-family interacting motif (AIM; or the LC3 interacting region), which binds to the AIM-binding pocket (AIMBP) of Atg8 family proteins (Noda et al., 2010; Johansen and Lamark, 2020). The P52 and R67 residues are located around the AIMBP, and an alanine substitution at these residues decreases the receptor-binding ability of Atg8 (Noda et al., 2008). Similar to *ATG11* knockout, this mutation also severely impaired autophagic degradation of GFP-tagged Nups (Fig. 2 B). These results suggest that a receptor-dependent mechanism mediates autophagic degradation of Nups.

Nups assembled into seven different NPC substructures were all degraded by autophagy (Fig. 1 B). In addition, their degradation was similarly affected by *ATG11* knockout and mutations in the AIMBP of Atg8 (Fig. 2, A and B). These results suggest that Nups are mainly sequestered into autophagosomes in the state of the NPC, while some Nups may also be degraded by autophagy in a form of assembly intermediates or unassembled proteins. Consistent with this prediction, immunoelectron microscopy detected signals of the pore filament component Nsp1 and the cytoplasmic filament component Nup159 (Nup159-HA) at electron-dense structures embedded in nuclear envelope–derived, double-membrane vesicles (see next section) within autophagic bodies, which are autophagosomal inner vesicles that accumulate within the vacuolar lumen in vacuolar protease-deficient cells (Takeshige et al., 1992; Fig. 2, C and D; and Fig. S1 C).

We previously reported that double-membrane vesicles form by budding from the nucleus and are selectively sequestered into autophagosomes in yeast cells treated with rapamycin (Mochida et al., 2015). This pathway is called "nucleophagy" and requires the outer nuclear membrane protein Atg39 as a specific receptor. Because Nups were found in double-membrane vesicles within autophagic bodies (Fig. 2, C and D), we predicted that nucleophagy was responsible for NPC degradation. Indeed, *ATG39* disruption decreased degradation of GFP-tagged Nups (Fig. 2 A). However, substantial amounts of GFP fragments were still observed in these cells. These results suggest that a proportion of the NPC is degraded via Atg39-dependent nucleophagy, but there exists another autophagy pathway for NPC degradation under TORC1-inactivating conditions. We also found autophagic bodies encapsulating Nsp1-positive double-membrane vesicles in *ATG39* knockout cells (Fig. S1 D), suggesting that an Atg39-independent mechanism also sequesters the NPC into autophagosomes in this manner.

We examined degradation of Nups in the absence of the other autophagy receptors Atg19, Atg32, Atg34, Atg36, Atg40, and Cue5, which are known to target vacuolar proteins, mitochondria, α-mannosidase, peroxisomes, the endoplasmic reticulum, and polyQ proteins, respectively (Fig. S2 A; Shintani et al., 2002; Kanki et al., 2009b; Okamoto et al., 2009; Suzuki et al., 2010; Motley et al., 2012; Lu et al., 2014; Mochida et al., 2015). Only *ATG40* knockout decreased Nup degradation. We previously reported that although Atg40 is a receptor for ER-phagy, a proportion of this protein resides in the nuclear envelope and that its absence partially impairs nucleophagy (Mochida et al., 2015). We also showed that *ATG40* knockout exacerbated defects in Nup degradation in *ATG39* knockout cells (Fig. S2 B). These results allowed us to speculate that Atg40 in the nuclear envelope, in addition to Atg39, participates in Nup degradation as a receptor. However, the AIM of Atg40 was dispensable for degradation of nuclear components, although it was strictly required for ER-phagy; its reticulon-like function probably promotes the formation of double-membrane vesicles in the nuclear envelope (our unpublished results). Thus, Atg40 is unlikely to act as a receptor in NPC degradation. We also compared degradation of Nups (Ndc1 and Nup85) with the inner nuclear membrane protein Src1, which was used to examine nucleophagy activity in our previous study (Mochida et al., 2015). *ATG39* knockout only partially affected degradation of the Nups but largely impaired that of Src1 (Fig. S2 B). Conversely, *ATG40* knockout had stronger effects on Nup degradation. These results suggest that the NPC and Nups are not merely degraded by nucleophagy as a bystander. In addition, our data showed that *ATG11* knockout and Atg8 AIMBP mutant cells exhibited more severe defects in NPC degradation than *ATG39* knockout cells (Fig. 2, A and B; and Fig. S2 C). These results suggest the

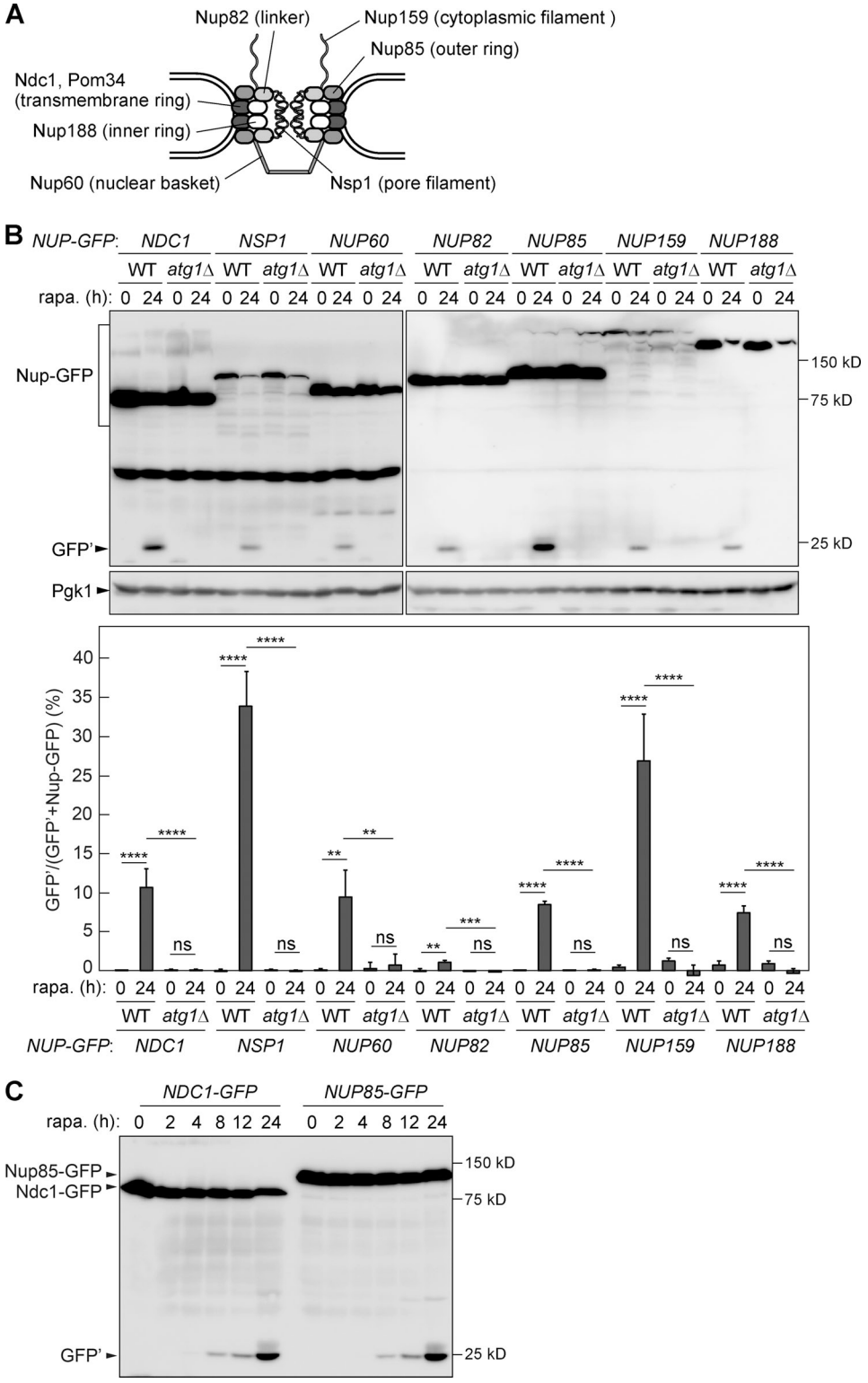

Figure 1. **Nups are degraded by autophagy in cells treated with rapamycin. (A)** The Nups analyzed in this study are shown in a schematic illustration of the NPC. **(B and C)** Degradation of GFP-fused Nup (Nup-GFP) by autophagy was analyzed by immunoblotting using an anti-GFP antibody before and after rapamycin (rapa.) treatment. GFP', GFP fragments generated by degradation of Nup-GFP in the vacuole. In B, the band intensities were quantified, and the proportions (%) of GFP' to the sum of GFP' and Nup-GFP are shown as means ± SD (n = 3). ns, not significant ($P \geq 0.05$); **, $P < 0.01$; ***, $P < 0.001$; ****, $P < 0.0001$ (Tukey's multiple comparisons test).

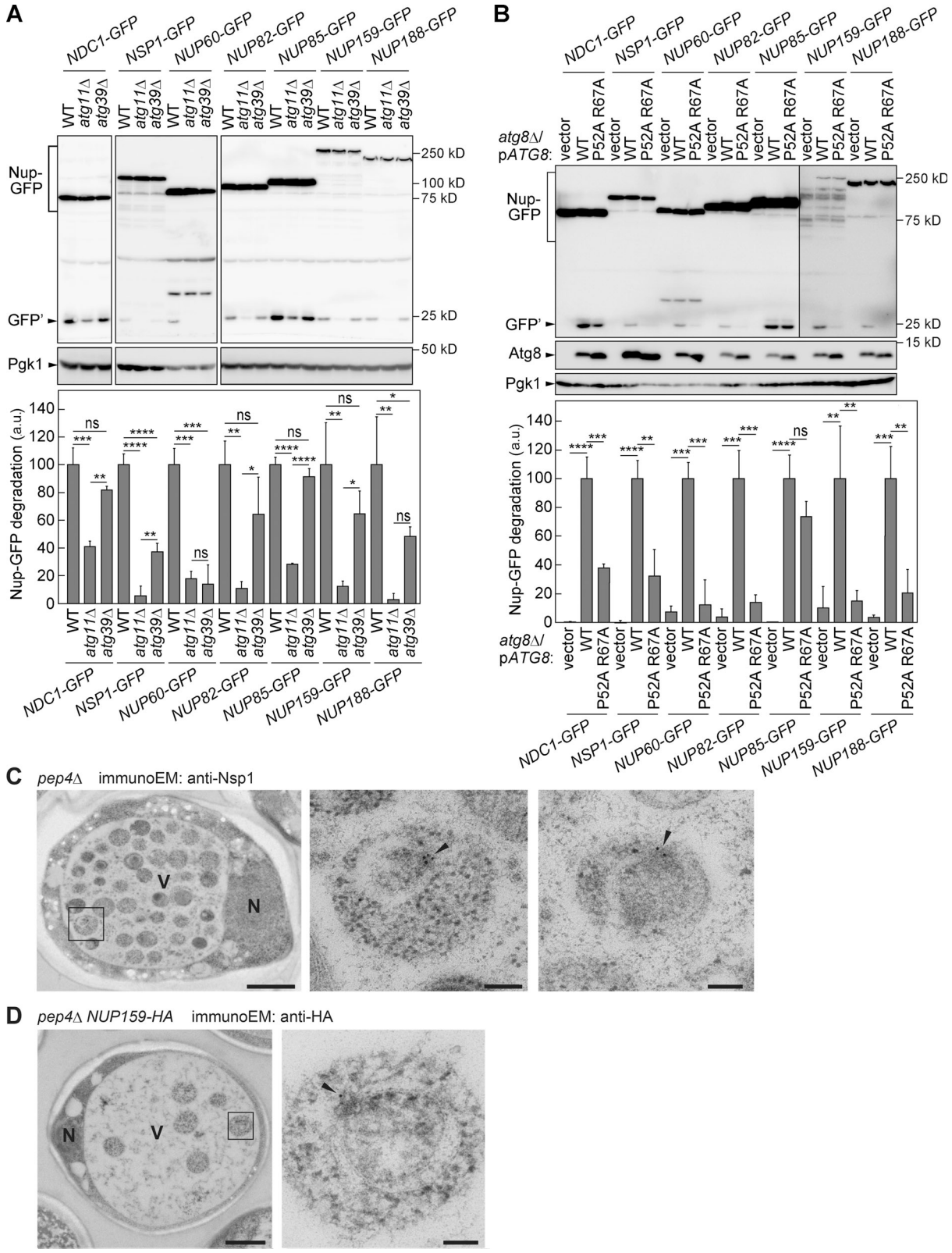

Figure 2. **Receptor-mediated selective autophagy degrades the NPC. (A)** WT, *atg11*Δ, and *atg39*Δ cells were treated with rapamycin for 24 h, and degradation of GFP-fused Nups was examined and measured as described in Fig. 1 B. In the quantification results, the values for WT cells were set to 100. Error bars represent SD (n = 3). ns, not significant (P ≥ 0.05); *, P < 0.05; **, P < 0.01; ***, P < 0.001; ****, P < 0.0001 (Tukey's multiple comparisons test). **(B)** *atg8*Δ cells expressing WT Atg8 or the AIM-binding pocket mutant (P52A R67A) from a single-copy plasmid were treated with rapamycin for 24 h, and degradation of GFP-fused Nups was examined and measured as described in A. Error bars represent SD (n = 3). ns, not significant (P ≥ 0.05); **, P < 0.01; ***, P < 0.001; ****, P < 0.0001 (Tukey's multiple comparisons test). **(C and D)** Immunoelectron microscopy of *pep4*Δ (C) and *pep4*Δ *NUP159-HA* (D) cells treated with rapamycin for

24 h was performed using anti-Nsp1 and anti-HA antibodies, respectively. The middle and right panels in C and D, respectively, are magnified view of the boxed area in the left panels. The right panel in C shows another example from a different area. Arrowheads indicate electron-dense regions containing Nsp1 or HA signals (gold particles) in double-membrane vesicles within autophagic bodies. Scale bars, 1 µm (left) and 100 nm (middle and right). V, vacuole. N, nucleus.

existence of an unknown receptor for an Atg39-independent degradation of the NPC.

We also showed that the sorting nexin Atg24, which is involved in selective autophagy pathways via an unknown mechanism (Nice et al., 2002; Kanki et al., 2009a; Shpilka et al., 2015; Nemec et al., 2017), is required for degradation of the NPC (Fig. S2 D). On the other hand, the absence of Nvj1, which is important for piecemeal microautophagy of the nucleus (Cadou and Mayer, 2015; Kvam and Goldfarb, 2007; Otto and Thumm, 2020), did not compromise NPC degradation (Fig. S2 E). This result is consistent with the observation that the NPC was excluded from the nucleus–vacuole junction, where piecemeal microautophagy of the nucleus occurs, in cells treated with rapamycin (Fig. S2 F and Fig. S1 A).

Nup159 interacts with Atg8 via the AIM

A number of selective autophagy substrates, such as fatty acid synthase, the clock repressor CRY1, and the nuclear receptor corepressor NCoR1, directly interact with Atg8 family proteins (Shpilka et al., 2015; Toledo et al., 2018; Saito et al., 2019). We found that the immunoprecipitation of FLAG-tagged Atg8 coprecipitated all of the HA-tagged Nups analyzed (Fig. 3 A). Moreover, almost all Nups were detected in immunoprecipitates of Atg8 by mass spectrometry (Table S1). These results suggest that the NPC interacts with Atg8. We showed that the NPC–Atg8 interaction depended on rapamycin treatment (Fig. 3 B). Moreover, the interaction was abolished by the mutation in the AIMBP of Atg8 (Fig. 3 C). These results suggest that an unknown AIM-containing protein mediates the interaction between the NPC and Atg8 upon TORC1 inactivation.

We hypothesized that the NPC binds to Atg8 via a Nup containing the AIM. Among putative AIM-containing proteins listed in the iLIR database (https://ilir.warwick.ac.uk; Jacomin et al., 2016), Nup159, Nup116, and Nup1 contain two, two, and one putative AIM, respectively (Fig. 4 A and Fig. S3 A). However, since coimmunoprecipitation of HA-tagged Nup1 with FLAG-Atg8 was not detected by immunoblotting (Fig. S3 B), Nup1 was excluded from further analysis. The core of the AIM is composed of four amino acid residues, in which aromatic and aliphatic residues at the first and fourth positions, respectively, are crucial for Atg8 binding (Noda et al., 2010; Johansen and Lamark, 2020). We replaced the first and fourth residues in the putative AIMs of Nup159 and Nup116 with alanine, expressed these mutants from plasmids in the presence of the chromosomally encoded WT proteins, and examined interactions of the mutant proteins with Atg8 by coimmunoprecipitation analysis (Fig. 4 A; and Fig. S3, A and B). The F443A L446A mutation in Nup159 and the two mutations in Nup116 did not impair the coprecipitation of these proteins with Atg8. By contrast, the Y1078A L1081A mutation in Nup159 reduced its coprecipitation with Atg8 to an undetectable level. (Although W303-derived strains were used in this study, the residue numbering of Nup159 is based on that in S288C-derived strains, because the *NUP159* gene from BY4741 was cloned and used for mutational analysis. Y1078 and L1081 correspond to Y1052 and L1055 of Nup159 in W303-derived strains, which lacks a part of the FG repeats.) We also constructed yeast strains expressing Nup159-GFP mutants in the absence of chromosomally encoded Nup159 and obtained similar results (Fig. 4 B). In addition, we showed that the coprecipitation of other Nups (Pom152 and Nsp1) with Atg8 was also impaired in Nup159$^{Y1078A\ L1081A}$ mutant cells (Fig. 4 B). Thus, the Y1078-D-K-L1081 sequence in Nup159 indeed functions as an AIM, and the interaction between Nup159 and Atg8 through this motif contributes considerably to the NPC–Atg8 interaction. We showed that knockout of *ATG39* and *ATG40* did not affect the interaction between Nup159 and Atg8 (Fig. S3 C).

The Nup159–Atg8 interaction mediates autophagic degradation of Nup159 not assembled into the NPC

Next, we examined the impact of the Nup159–Atg8 interaction on autophagic degradation of the NPC. Fluorescence microscopy confirmed that the Nup159-GFP mutants localized to the nuclear envelope, similar to WT Nup159-GFP (Fig. 4 C and Fig. S3 D). The GFP processing assay revealed that whereas Nup159$^{F443A\ L446A}$-GFP was degraded by autophagy comparably to WT Nup159-GFP, Nup159$^{Y1078A\ L1081A}$-GFP exhibited a significant defect in its degradation (Fig. 4 D and Fig. S3 E). However, other Nups we tested were all degraded normally in Nup159$^{Y1078A\ L1081A}$ mutant cells (Fig. 4 E). These results suggest that while Nup159 interacts with Atg8 via the AIM both inside and outside of the NPC, the interaction of Nup159 with Atg8 is important for degradation of this Nup itself, but not for that of the whole NPC. Nonetheless, it is still possible that the Nup159–Atg8 interaction is also involved in degradation of the whole NPC along with other interactions that link the NPC to Atg8, including an interaction mediated by an unknown receptor.

In this study, we provided the first evidence for autophagic degradation of the NPC and Nups, which we term "NPC-phagy" and "nucleoporinophagy," respectively. Our results suggest that multiple selective autophagy pathways mediate NPC/Nup degradation in *S. cerevisiae* cells when TORC1 activity is attenuated. Immunoelectron microscopy revealed that NPCs in the state of being embedded in nuclear envelope–derived, double-membrane vesicles are enclosed within autophagosomes (Fig. 5 A). Atg39-dependent nucleophagy is likely to participate in NPC degradation in this manner.

In addition, our results suggested the existence of an unknown receptor, which might be specific to NPC-phagy and function in collaboration with Atg11. Although we have been unable to identify such a receptor to date, we found that the cytoplasmic filament component Nup159 interacts with Atg8 via the AIM and that this interaction is pivotal for the NPC association with Atg8. Given these results, we predicted that autophagic degradation of the NPC was affected by the mutation in

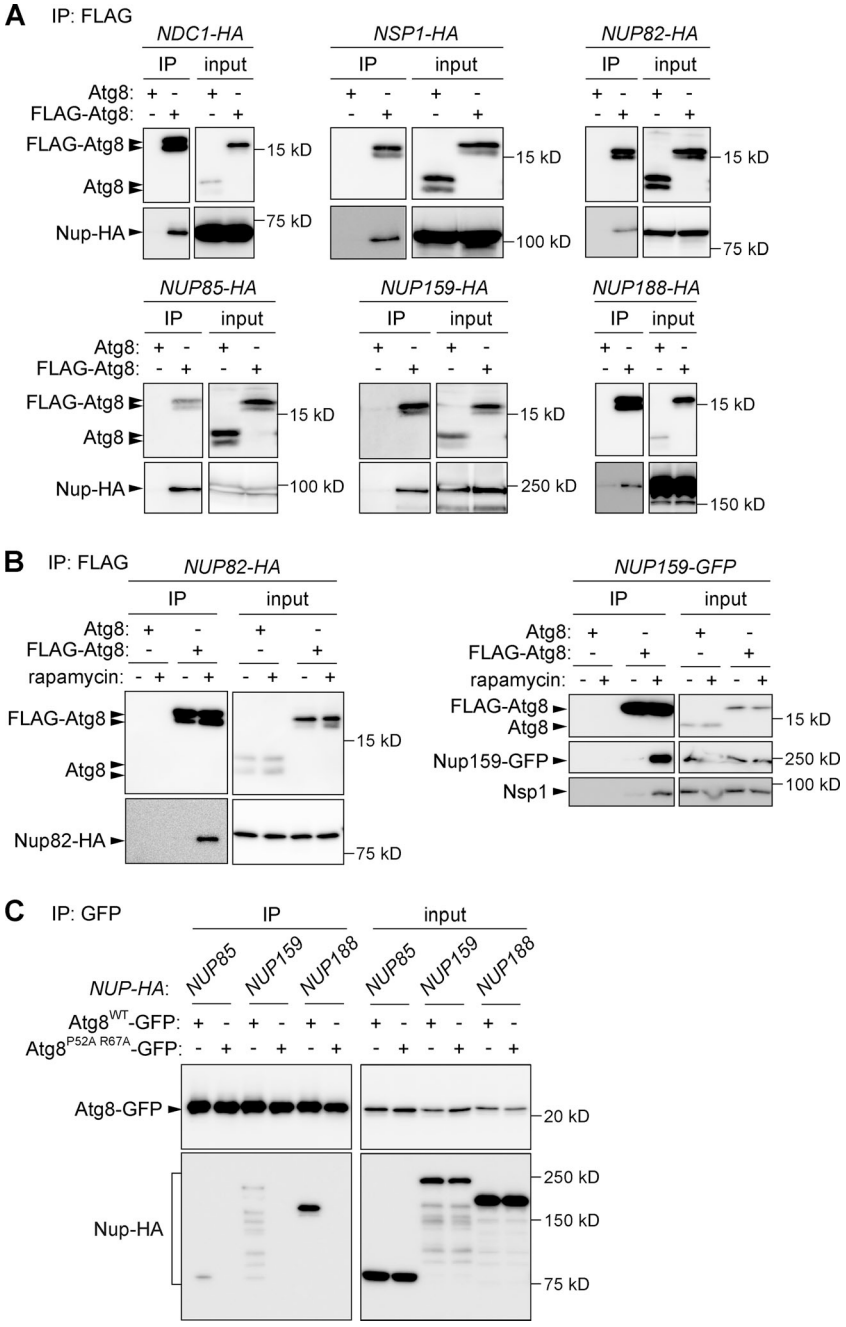

Figure 3. **The NPC associates with Atg8 upon rapamycin treatment depending on the receptor-binding ability of Atg8. (A)** Cells expressing 3×FLAG-tagged Atg8 (FLAG-Atg8) and 6×HA-tagged Nups (Nup-HA) were treated with rapamycin for 2 h. Cell lysates (input) were subjected to immunoprecipitation using an anti-FLAG antibody, and the immunoprecipitates (IP) were analyzed by immunoblotting using antibodies against Atg8 and HA. **(B)** Immunoprecipitation was performed for cells treated with or without rapamycin as described in A, followed by immunoblotting using antibodies against Atg8, HA, GFP, and Nsp1. **(C)** *atg8*Δ cells carrying a single-copy plasmid for the expression of $Atg8^{WT}$-GFP or $Atg8^{P52A\ R67A}$-GFP were treated with rapamycin for 2 h and used for immunoprecipitation with an anti-GFP antibody and subsequent immunoblotting with anti-Atg8 and anti-HA antibodies.

the AIM of Nup159. However, although this mutation significantly retarded degradation of the Nup159 mutant itself, it did not influence degradation of other Nups. These results were contrary to our expectation but clearly showed that Nups not assembled into the NPC can also be targets for selective autophagy (nucleoporinophagy; Fig. 5 B). In the case of Nup159, binding to Atg8 via the AIM contributes to its efficient degradation. We observed cytoplasmic puncta of Nup159-GFP (Fig. 4 C and Fig. S3 D), allowing us to speculate that aggregates of Nup159 or Nup159-containing subcomplexes are taken up by autophagosomes via the interaction with Atg8. Unassembled Nup159 or Nup159 dissociated from the NPC may be directed to autophagic elimination to control the integrity or function of the NPC under TORC1-inactivating conditions. A previous study reported that monoubiquitylated Nup159 recruits the dynein light chain to the NPC, which is important for nuclear segregation during mitosis (Hayakawa et al., 2012). Therefore, it is possible that autophagic degradation of Nup159 is involved in the control of cell cycle progression. Other Nups may also be subjected to nucleoporinophagy by binding to Atg8 or unknown receptors under certain conditions.

NPC-phagy can contribute to the control of the quality and quantity of the whole NPC. TORC1 inhibition evokes different cellular responses, including autophagy, and causes cell cycle arrest at G1 phase with delayed G2/M transition (Loewith and Hall, 2011; Barbet et al., 1996; Nakashima et al., 2008). In *S. cerevisiae*, the nuclear envelope and NPCs are not disassembled during mitosis, and NPC assembly occurs continuously throughout

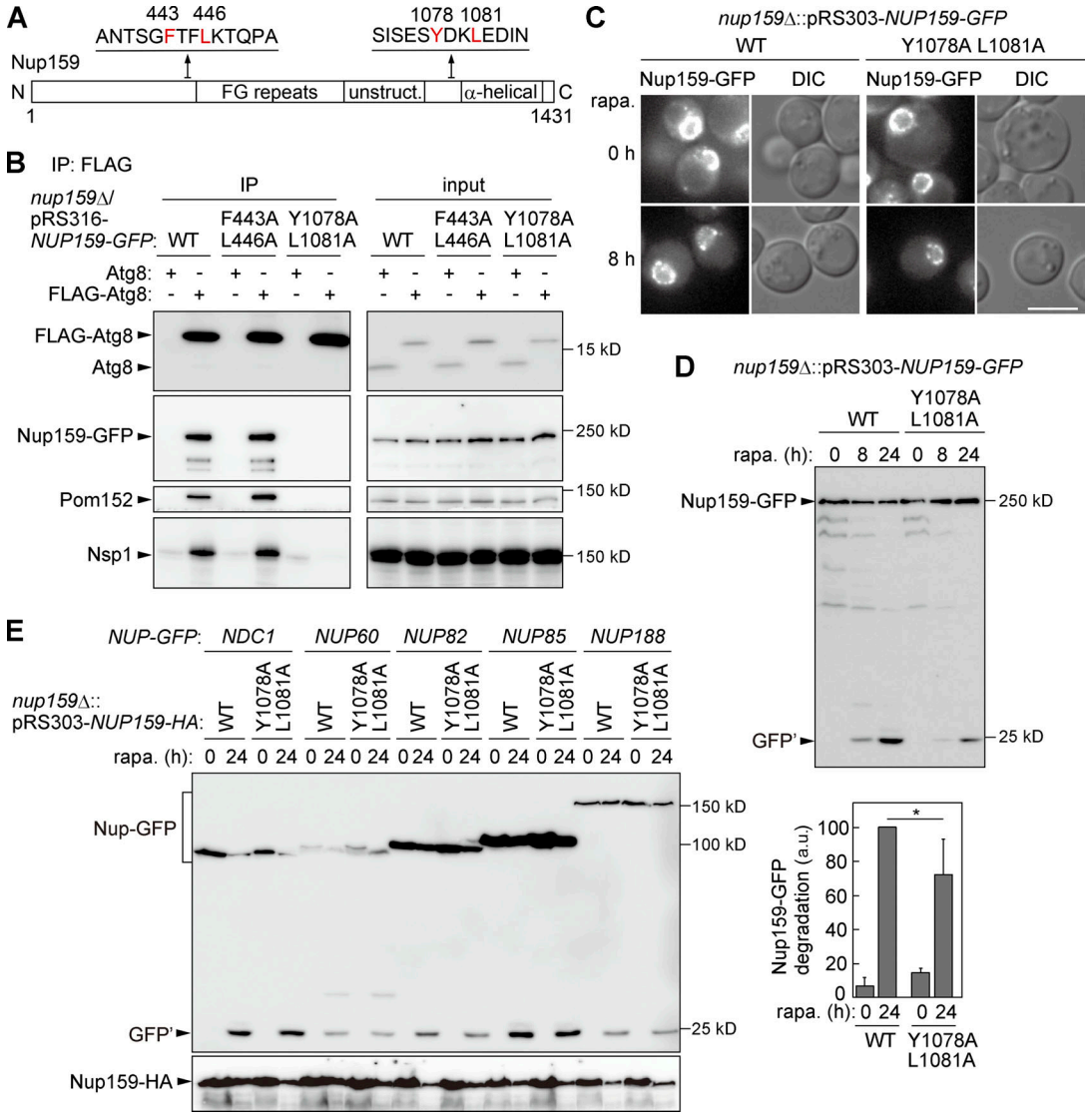

Figure 4. **Autophagic degradation of Nup159 via its AIM-mediated interaction with Atg8. (A)** Schematic diagram of the domain architecture of Nup159. The functional AIM (Y1078-D-K-L1081) lies between the unstructured (unstruct) and α-helical regions. **(B)** *nup159Δ* cells carrying *NUP159-GFP* single-copy plasmids were treated with rapamycin for 2 h and subjected to immunoprecipitation using an anti-FLAG antibody. The immunoprecipitates were analyzed by immunoblotting using antibodies against Atg8, GFP, Pom152, and Nsp1. **(C)** Cells expressing Nup159-GFP and the Y1078A L1081A mutant were treated with rapamycin and observed under a fluorescence microscope. DIC, differential interference contrast microscopy. Scale bar, 5 µm. **(D)** Autophagic degradation of Nup159-GFP in the same strains as those used in C was examined and quantified as described in Fig. 2 A. Error bars represent SD (n = 3). *, $P < 0.05$ (Tukey's multiple comparisons test). **(E)** Autophagic degradation of GFP-tagged Nups in Nup159$^{Y1078A\ L1081A}$ mutant cells was examined as described in Fig. 1 B.

the cell cycle (Winey et al., 1997). NPC-phagy may promote NPC turnover or remove misassembled/malfunctioned NPCs and thereby participate in the maintenance of the NPC under TORC1-inactivating conditions. Consistent with this idea, disruption of *NUP116*, which destabilizes the NPC (Onischenko et al., 2017), stimulated autophagic degradation of the NPC (Fig. S3 F). In other organisms in which NPC disassembly occurs and Nups are dispersed in the cytoplasm during cell division, some Nups may be degraded by nucleoporinophagy.

During the course of this study, another group also reported that NPCs are degraded by selective autophagy under nitrogen starvation in *S. cerevisiae* and that this NPC degradation was enhanced by the absence of Nups (Nup120 and Nup133) that cause aberrant NPC clustering in the nuclear envelope (Lee et al., 2020). However, there are some contradictory results between the two studies. The same AIM in Nup159 has also been identified in that study, but unlike our results, the AIM mutation significantly reduced degradation of other Nups, and accordingly, Nup159 has been proposed as an autophagy receptor for NPC degradation. In addition, deletion of *NUP116* rather impeded autophagy of the NPC (Lee et al., 2020). These discrepancies might be due to different strain backgrounds used in the two studies, but close examination will be required to resolve this issue.

The NPC has been implicated in the replicative life span of *S. cerevisiae* (Lord et al., 2015). In addition, a deficiency in the NPC leads to various human diseases and aging (Nofrini et al., 2016;

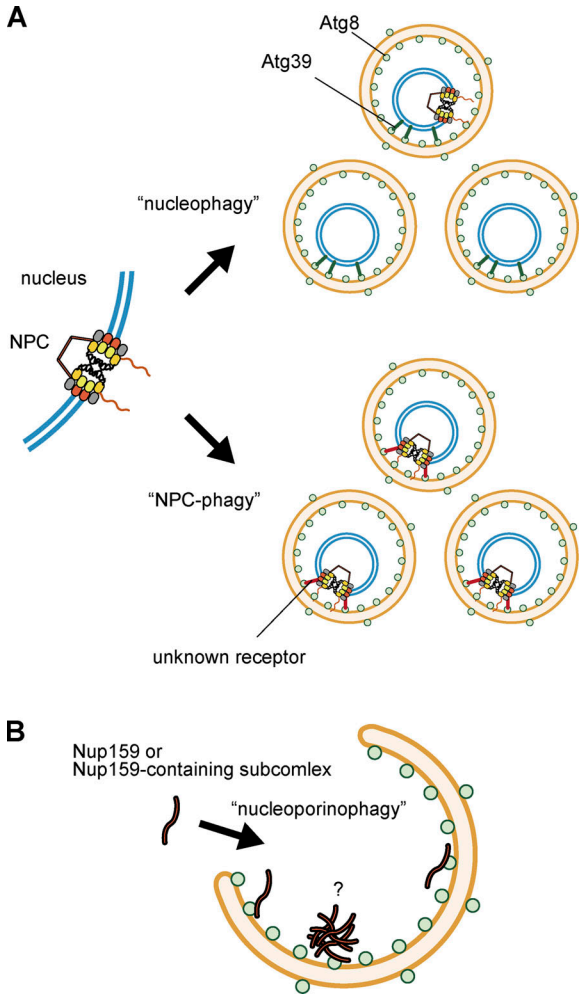

Figure 5. **Working model for NPC-phagy and nucleoporinophagy. (A)** Under TORC1-inactivating conditions, the NPC is loaded into double-membrane vesicles budded from the nuclear envelope, and these vesicles are sequestered into autophagosomes via Atg39-dependent nucleophagy and another pathway mediated by an unknown autophagy receptor. **(B)** Nup159, a cytoplasmic filament component of the NPC, is captured by autophagosomes via the interaction with Atg8, when it exists in the cytoplasm without integration into the NPC.

Sakuma and D'Angelo, 2017). The basic framework for understanding NPC-phagy and nucleoporinophagy determined in this study provides a foundation for studies of the molecular mechanisms and physiological/pathological significance of these new autophagy pathways in various organisms.

Materials and methods

Yeast strains and media

Yeast strains used in this study were derived from W303-1A or BJ2168 (Thomas and Rothstein, 1989; Jones, 1991) and are listed in Table S2. Gene disruption and tagging were performed by a standard method (Janke et al., 2004). Yeast cells were grown at 30°C in YPD medium (1% yeast extract, 2% peptone, and 2% glucose) or SD+CA+ATU medium (0.17% yeast nitrogen base without amino acids and ammonium sulfate, 0.5% casamino acid, 2% glucose, 0.002% adenine sulfate, 0.002% tryptophan, and 0.002% uracil). SD+CA+ATU without uracil (SD+CA+AT) was used for the culture of strains carrying pRS316-derived plasmids. To induce autophagy, cells grown to mid-log phase were treated with 200 ng/ml rapamycin or incubated in SD-N medium (0.17% yeast nitrogen base without amino acids and ammonium sulfate and 2% glucose).

Plasmids

pRS316-based centromeric plasmids for the expression of $Atg8^{WT}$ and $Atg8^{P52A\ R67A}$, $Atg8^{G116A}$–GFP, and $Atg8^{P52A\ R67A\ G116A}$–GFP were described previously (Mochida et al., 2015; used in Fig. 2 B, Fig. 3 C, and Fig. S2 C). pRS316-*NUP159-GFP*, pRS316-*NUP1-6×HA*, and pRS316-*NUP116-6×HA* (used in Fig. 4 B and Fig. S3, B, D, and E) were constructed as follows. The coding sequences of *NUP159-GFP*, *NUP1-6×HA*, and *NUP116-6×HA* with their original promoters were amplified by PCR using genomic DNA prepared from YTY171, YTY304, and YTY309 (Table S2). The PCR products were cloned into pRS316 using the Gibson Assembly Kit (New England Biolabs). Point mutations were introduced into these plasmids by a PCR-based method. To introduce mutations into *NUP159* on genomic DNA, 2,415–4,302 bp of the *NUP159* ORF followed by the GFP or 6×HA sequence as well as this DNA fragment containing the Y1078A L1081A mutation were cloned into pRS303 together with the *PGK1* terminator using the Gibson Assembly Kit, yielding pRS303-$NUP159^{2415\text{-}4302bp}$-*GFP/6×HA* and pRS303-$NUP159^{2415\text{-}4302bp\ Y1078A\ L1081A}$-*GFP/6×HA*. These plasmids were digested within the *NUP159* sequence by SpeI and introduced into yeast cells for integration into the *NUP159* locus by homologous recombination to obtain the strains used for the analyses shown in Fig. 4, C, D, and E.

Immunoblotting

For immunoblotting, antibodies against GFP (632381; Clontech), Atg8 (Nakatogawa et al., 2012), HA (11867423001; Roche), Nsp1, and Pom152 (gifts from Dr. Tohru Yoshihisa, University of Hyogo, Hyogo, Japan) were used. To prepare the samples for the Nup–GFP processing assay, yeast cell pellets were suspended in 0.1 M NaOH, kept on ice for 5 min, and centrifuged at 5,000 rpm for 5 min at 4°C. The pellets were suspended in Urea SDS sample buffer (37.5 mM MOPS-NaOH, pH 6.8, 2% SDS, 100 mM DTT, 4 M urea, and a trace amount of bromophenol blue) and incubated at 65°C for 10 min. These samples were centrifuged at 15,000 *g* for 1 min, and the supernatants were subjected to SDS-PAGE and immunoblotting.

Immunoprecipitation

Yeast cells grown to mid-log phase were converted to spheroplasts by incubating them in 0.5× YPD or 0.5× SD+CA+AT medium containing 1 M sorbitol and 10 U/OD_{600}-unit-cells zymolyase 100T (Nacalai Tesque). The spheroplasts were washed with 20 mM Hepes-KOH (pH 7.2) and 1.2 M sorbitol, treated with 200 ng/ml rapamycin (LC Laboratories) in 0.5× YPD or 0.5× SD+CA+AT medium containing 1 M sorbitol for 2 h at 30°C, and lysed with IP buffer (50 mM Tris-HCl, pH 8.0, 150 mM NaCl, 10% glycerol, and 5 mM EDTA) containing 2× cOmplete Protease Inhibitor Cocktail (Roche), 2 mM phenylmethylsulfonyl fluoride, and 1.0% *n*-dodecyl-β-D-maltoside for 30 min at 4°C. The cell lysates were centrifuged at 15,000 *g* for 15 min, and the

supernatants were incubated with NHS FG-beads (Tamagawa Seiki) conjugated with anti-FLAG M2 antibody (F1804; Sigma-Aldrich) or GFP Nanobody (Harada et al., 2019) at 4°C for 2 h. The beads were washed with IP buffer containing 0.1% *n*-dodecyl-β-D-maltoside three times and then incubated in Urea SDS sample buffer at 65°C for 10 min to elute bound proteins.

Fluorescence microscopy

Fluorescence microscopy to confirm the nuclear localization of GFP-tagged Nups was performed using an inverted fluorescence microscope (IX83; Olympus) equipped with a 488-nm laser, electron multiplying charge-coupled device camera, and a 150× objective lens as described previously (Kotani et al., 2018). Images were acquired using MetaMorph (Molecular Devices) and processed using Fiji (ImageJ; Schneider et al., 2012; Schindelin et al., 2012).

Electron microscopy

Electron microscopy was performed by Tokai-EMA based on rapid freezing and freeze-fixation methods. Cells were sandwiched with copper disks and quickly frozen in liquid propane at −175°C. The frozen samples were substituted with 1% tannic acid in ethanol and 2% distilled water at −80°C for 48 h and then and kept at −20°C for 4 h and at 4°C for 1 h. These samples were dehydrated in anhydrous ethanol for 30 min three times and infiltrated with a 50:50 mixture of ethanol and LR white resin (London Resin) at 4°C for 1 h. After infiltration, the samples were washed with LR white three times by incubation at 4°C for 30 min for each wash process and transferred to fresh LR white, followed by polymerization at 50°C overnight. The polymerized resins were ultrathin sectioned, and the sections were placed on nickel grids and immunostained with anti-Nsp1 antibodies and secondary antibodies conjugated to 10-nm gold particles as reported previously (Shima et al., 2019). Electron microscopy was performed using a transmission electron microscope (JEM-1400Plus; JEOL), and digital images (3,296 × 2,472 pixels) were obtained using a charge-coupled device camera (EM-14830RUBY2; JEOL).

Mass spectrometry of Atg8 immunoprecipitates

Yeast cells expressing 3×FLAG-tagged Atg8 (FLAG-Atg8) or nontagged Atg8 were spheroplasted, treated with rapamycin, and subjected to immunoprecipitation using an anti-FLAG antibody as described in Materials and methods. The resulting immunoprecipitates were analyzed by mass spectrometry. Identified proteins with a normalized abundance in samples from FLAG-Atg8 cells that is fivefold higher than that in samples from nontagged Atg8 cells were selected, and Nups, proteins involved in autophagosome formation (autophagy machinery), known substrates, or receptors for selective autophagy (autophagy substrate/receptor) are listed in Table S1.

Online supplemental material

Fig. S1 shows the results related to autophagic degradation of Nups. Fig. S2 shows the results of Nup degradation in various autophagy-related mutants. Fig. S3 shows the results of the analysis of Nup mutants. Table S1 shows the results of mass spectrometry of Atg8 immunoprecipitates. Table S2 lists the yeast strains used in this study.

Acknowledgments

We thank the members of our laboratories for materials, discussions, and technical and secretarial support. We also thank Dr. Tohru Yoshihisa for antibodies against Nsp1 and Pom152 and the Biomaterial Analysis Center, Technical Department at Tokyo Institute of Technology for DNA sequencing services.

This work was supported in part by the Ministry of Education, Culture, Sports, Science, and Technology (KAKENHI Grants-in-Aid for Scientific Research 25111003, 17H01430, and 19H05708 to H. Nakatogawa), the Japan Science and Technology Agency (CREST grant JPMJCR13M7 to H. Nakatogawa), the Tokyo Tech Fund (STAR grant to H. Nakatogawa), and the NOVARTIS Foundation (Japan) for the Promotion of Science (to H. Nakatogawa).

The authors declare no competing financial interests.

Author contributions: Y. Tomioka, T. Kotani, Y. Ohsumi, and H. Nakatogawa designed the project. Y. Tomioka performed most of the experiments with the help of H. Kirisako. Y. Oikawa, Y. Kimura, and H. Hirano performed mass spectrometry analysis. Y. Tomioka and H. Nakatogawa wrote the manuscript. All authors analyzed and discussed the results and commented on the manuscript.

Submitted: 22 October 2019
Revised: 5 March 2020
Accepted: 20 April 2020

References

Aitchison, J.D., and M.P. Rout. 2012. The yeast nuclear pore complex and transport through it. *Genetics*. 190:855–883. https://doi.org/10.1534/genetics.111.127803

Barbet, N.C., U. Schneider, S.B. Helliwell, I. Stansfield, M.F. Tuite, and M.N. Hall. 1996. TOR controls translation initiation and early G1 progression in yeast. *Mol. Biol. Cell*. 7:25–42. https://doi.org/10.1091/mbc.7.1.25

Cadou, A., and A. Mayer. 2015. The Nucleus-Vacuole Junction in Saccharomyces Cerevisiae. *In Autophagy: Cancer, Other Pathologies, Inflammation, Immunity, Infection, and Aging*. M. Hayat, editor. Academic Press, New York. pp. 69–77. https://doi.org/10.1016/B978-0-12-801043-3.00003-0

Gatica, D., V. Lahiri, and D.J. Klionsky. 2018. Cargo recognition and degradation by selective autophagy. *Nat. Cell Biol*. 20:233–242. https://doi.org/10.1038/s41556-018-0037-z

Harada, K., T. Kotani, H. Kirisako, M. Sakoh-Nakatogawa, Y. Oikawa, Y. Kimura, H. Hirano, H. Yamamoto, Y. Ohsumi, and H. Nakatogawa. 2019. Two distinct mechanisms target the autophagy-related E3 complex to the pre-autophagosomal structure. *eLife*. 8. e43088. https://doi.org/10.7554/eLife.43088

Hayakawa, A., A. Babour, L. Sengmanivong, and C. Dargemont. 2012. Ubiquitylation of the nuclear pore complex controls nuclear migration during mitosis in S. cerevisiae. *J. Cell Biol*. 196:19–27. https://doi.org/10.1083/jcb.201108124

Jacomin, A.C., S. Samavedam, V. Promponas, and I.P. Nezis. 2016. iLIR database: A web resource for LIR motif-containing proteins in eukaryotes. *Autophagy*. 12:1945–1953. https://doi.org/10.1080/15548627.2016.1207016

Janke, C., M.M. Magiera, N. Rathfelder, C. Taxis, S. Reber, H. Maekawa, A. Moreno-Borchart, G. Doenges, E. Schwob, E. Schiebel, et al. 2004. A versatile toolbox for PCR-based tagging of yeast genes: new fluorescent proteins, more markers and promoter substitution cassettes. *Yeast*. 21:947–962. https://doi.org/10.1002/yea.1142

Johansen, T., and T. Lamark. 2020. Selective Autophagy: ATG8 Family Proteins, LIR Motifs and Cargo Receptors. *J. Mol. Biol*. 432:80–103. Available at: PubMed. https://doi.org/10.1016/j.jmb.2019.07.016

Jones, E.W.. 1991. Tackling the protease problem in Saccharomyces cerevisiae. *Methods Enzymol*. 194:428–453. https://doi.org/10.1016/0076-6879(91)94034-A

Kanki, T., K. Wang, M. Baba, C.R. Bartholomew, M.A. Lynch-Day, Z. Du, J. Geng, K. Mao, Z. Yang, W.L. Yen, and D.J. Klionsky. 2009a. A genomic screen for yeast mutants defective in selective mitochondria autophagy. *Mol. Biol. Cell*. 20:4730–4738. https://doi.org/10.1091/mbc.e09-03-0225

Kanki, T., K. Wang, Y. Cao, M. Baba, and D.J. Klionsky. 2009b. Atg32 is a mitochondrial protein that confers selectivity during mitophagy. *Dev. Cell*. 17:98–109. https://doi.org/10.1016/j.devcel.2009.06.014

Kim, S.J., J. Fernandez-Martinez, I. Nudelman, Y. Shi, W. Zhang, B. Raveh, T. Herricks, B.D. Slaughter, J.A. Hogan, P. Upla, et al. 2018. Integrative structure and functional anatomy of a nuclear pore complex. *Nature*. 555:475–482. https://doi.org/10.1038/nature26003

Kirkin, V.. 2020. History of the Selective Autophagy Research: How Did It Begin and Where Does It Stand Today? *J. Mol. Biol*. 432:3–27. https://doi.org/10.1016/j.jmb.2019.05.010

Kotani, T., H. Kirisako, M. Koizumi, Y. Ohsumi, and H. Nakatogawa. 2018. The Atg2-Atg18 complex tethers pre-autophagosomal membranes to the endoplasmic reticulum for autophagosome formation. *Proc. Natl. Acad. Sci. USA*. 115:10363–10368. https://doi.org/10.1073/pnas.1806727115

Kvam, E., and D.S. Goldfarb. 2007. Nucleus-vacuole junctions and piecemeal microautophagy of the nucleus in S. cerevisiae. *Autophagy*. 3:85–92. https://doi.org/10.4161/auto.3586

Lee, C.W., F. Wilfling, P. Ronchi, M. Allegretti, S. Mosalaganti, S. Jentsch, M. Beck, and B. Pfander. 2020. Selective autophagy degrades nuclear pore complexes. *Nat. Cell Biol*. 22:159–166. https://doi.org/10.1038/s41556-019-0459-2

Loewith, R., and M.N. Hall. 2011. Target of rapamycin (TOR) in nutrient signaling and growth control. *Genetics*. 189:1177–1201. https://doi.org/10.1534/genetics.111.133363

Loewith, R., E. Jacinto, S. Wullschleger, A. Lorberg, J.L. Crespo, D. Bonenfant, W. Oppliger, P. Jenoe, and M.N. Hall. 2002. Two TOR complexes, only one of which is rapamycin sensitive, have distinct roles in cell growth control. *Mol. Cell*. 10:457–468. https://doi.org/10.1016/S1097-2765(02)00636-6

Lord, C.L., B.L. Timney, M.P. Rout, and S.R. Wente. 2015. Altering nuclear pore complex function impacts longevity and mitochondrial function in S. cerevisiae. *J. Cell Biol*. 208:729–744. https://doi.org/10.1083/jcb.201412024

Lu, K., I. Psakhye, and S. Jentsch. 2014. Autophagic clearance of polyQ proteins mediated by ubiquitin-Atg8 adaptors of the conserved CUET protein family. *Cell*. 158:549–563. https://doi.org/10.1016/j.cell.2014.05.048

Matsuura, A., M. Tsukada, Y. Wada, and Y. Ohsumi. 1997. Apg1p, a novel protein kinase required for the autophagic process in Saccharomyces cerevisiae. *Gene*. 192:245–250. https://doi.org/10.1016/S0378-1119(97)00084-X

Mochida, K., Y. Oikawa, Y. Kimura, H. Kirisako, H. Hirano, Y. Ohsumi, and H. Nakatogawa. 2015. Receptor-mediated selective autophagy degrades the endoplasmic reticulum and the nucleus. *Nature*. 522:359–362. https://doi.org/10.1038/nature14506

Motley, A.M., J.M. Nuttall, and E.H. Hettema. 2012. Pex3-anchored Atg36 tags peroxisomes for degradation in Saccharomyces cerevisiae. *EMBO J*. 31:2852–2868. https://doi.org/10.1038/emboj.2012.151

Nakashima, A., Y. Maruki, Y. Imamura, C. Kondo, T. Kawamata, I. Kawanishi, H. Takata, A. Matsuura, K.S. Lee, U. Kikkawa, et al. 2008. The yeast Tor signaling pathway is involved in G2/M transition via polo-kinase. *PLoS One*. 3. e2223. https://doi.org/10.1371/journal.pone.0002223

Nakatogawa, H., J. Ishii, E. Asai, and Y. Ohsumi. 2012. Atg4 recycles inappropriately lipidated Atg8 to promote autophagosome biogenesis. *Autophagy*. 8:177–186. https://doi.org/10.4161/auto.8.2.18373

Nemec, A.A., L.A. Howell, A.K. Peterson, M.A. Murray, and R.J. Tomko, Jr.. 2017. Autophagic clearance of proteasomes in yeast requires the conserved sorting nexin Snx4. *J. Biol. Chem*. 292:21466–21480. https://doi.org/10.1074/jbc.M117.817999

Nice, D.C., T.K. Sato, P.E. Stromhaug, S.D. Emr, and D.J. Klionsky. 2002. Cooperative binding of the cytoplasm to vacuole targeting pathway proteins, Cvt13 and Cvt20, to phosphatidylinositol 3-phosphate at the pre-autophagosomal structure is required for selective autophagy. *J. Biol. Chem*. 277:30198–30207. https://doi.org/10.1074/jbc.M204736200

Noda, T., and Y. Ohsumi. 1998. Tor, a phosphatidylinositol kinase homologue, controls autophagy in yeast. *J. Biol. Chem*. 273:3963–3966. https://doi.org/10.1074/jbc.273.7.3963

Noda, N.N., H. Kumeta, H. Nakatogawa, K. Satoo, W. Adachi, J. Ishii, Y. Fujioka, Y. Ohsumi, and F. Inagaki. 2008. Structural basis of target recognition by Atg8/LC3 during selective autophagy. *Genes Cells*. 13:1211–1218. https://doi.org/10.1111/j.1365-2443.2008.01238.x

Noda, N.N., Y. Ohsumi, and F. Inagaki. 2010. Atg8-family interacting motif crucial for selective autophagy. *FEBS Lett*. 584:1379–1385. https://doi.org/10.1016/j.febslet.2010.01.018

Nofrini, V., D. Di Giacomo, and C. Mecucci. 2016. Nucleoporin genes in human diseases. *Eur. J. Hum. Genet*. 24:1388–1395. https://doi.org/10.1038/ejhg.2016.25

Ohsumi, Y.. 2014. Historical landmarks of autophagy research. *Cell Res*. 24:9–23. https://doi.org/10.1038/cr.2013.169

Okamoto, K., N. Kondo-Okamoto, and Y. Ohsumi. 2009. Mitochondria-anchored receptor Atg32 mediates degradation of mitochondria via selective autophagy. *Dev. Cell*. 17:87–97. https://doi.org/10.1016/j.devcel.2009.06.013

Onischenko, E., J.H. Tang, K.R. Andersen, K.E. Knockenhauer, P. Vallotton, C.P. Derrer, A. Kralt, C.F. Mugler, L.Y. Chan, T.U. Schwartz, et al. 2017. Natively Unfolded FG Repeats Stabilize the Structure of the Nuclear Pore Complex. *Cell*. 171:904–917.e19. https://doi.org/10.1016/j.cell.2017.09.033

Otto, F.B., and M. Thumm. 2020. Mechanistic dissection of macro- and micronucleophagy. *Autophagy*. 1–14. https://doi.org/10.1080/15548627.2020.1725402

Rajoo, S., P. Vallotton, E. Onischenko, and K. Weis. 2018. Stoichiometry and compositional plasticity of the yeast nuclear pore complex revealed by quantitative fluorescence microscopy. *Proc. Natl. Acad. Sci. USA*. 115:E3969–E3977. https://doi.org/10.1073/pnas.1719398115

Saito, T., A. Kuma, Y. Sugiura, Y. Ichimura, M. Obata, H. Kitamura, S. Okuda, H.C. Lee, K. Ikeda, Y. Kanegae, et al. 2019. Autophagy regulates lipid metabolism through selective turnover of NCoR1. *Nat. Commun*. 10:1567. https://doi.org/10.1038/s41467-019-08829-3

Sakuma, S., and M.A. D'Angelo. 2017. The roles of the nuclear pore complex in cellular dysfunction, aging and disease. *Semin. Cell Dev. Biol*. 68:72–84. https://doi.org/10.1016/j.semcdb.2017.05.006

Schindelin, J., I. Arganda-Carreras, E. Frise, V. Kaynig, M. Longair, T. Pietzsch, S. Preibisch, C. Rueden, S. Saalfeld, B. Schmid, et al. 2012. Fiji: an open-source platform for biological-image analysis. *Nat. Methods*. 9:676–682. https://doi.org/10.1038/nmeth.2019

Schneider, C.A., W.S. Rasband, and K.W. Eliceiri. 2012. NIH Image to ImageJ: 25 years of image analysis. *Nat. Methods*. 9:671–675. https://doi.org/10.1038/nmeth.2089

Shima, T., H. Kirisako, and H. Nakatogawa. 2019. COPII vesicles contribute to autophagosomal membranes. *J. Cell Biol*. 218:1503–1510. https://doi.org/10.1083/jcb.201809032

Shintani, T., W.P. Huang, P.E. Stromhaug, and D.J. Klionsky. 2002. Mechanism of cargo selection in the cytoplasm to vacuole targeting pathway. *Dev. Cell*. 3:825–837. https://doi.org/10.1016/S1534-5807(02)00373-8

Shpilka, T., E. Welter, N. Borovsky, N. Amar, F. Shimron, Y. Peleg, and Z. Elazar. 2015. Fatty acid synthase is preferentially degraded by autophagy upon nitrogen starvation in yeast. *Proc. Natl. Acad. Sci. USA*. 112:1434–1439. https://doi.org/10.1073/pnas.1409476112

Strambio-De-Castillia, C., M. Niepel, and M.P. Rout. 2010. The nuclear pore complex: bridging nuclear transport and gene regulation. *Nat. Rev. Mol. Cell Biol*. 11:490–501. https://doi.org/10.1038/nrm2928

Suzuki, K., C. Kondo, M. Morimoto, and Y. Ohsumi. 2010. Selective transport of α-mannosidase by autophagic pathways: identification of a novel receptor, Atg34p. *J. Biol. Chem*. 285:30019–30025. https://doi.org/10.1074/jbc.M110.143511

Takeshige, K., M. Baba, S. Tsuboi, T. Noda, and Y. Ohsumi. 1992. Autophagy in yeast demonstrated with proteinase-deficient mutants and conditions for its induction. *J. Cell Biol*. 119:301–311. https://doi.org/10.1083/jcb.119.2.301

Thomas, B.J., and R. Rothstein. 1989. Elevated recombination rates in transcriptionally active DNA. *Cell*. 56:619–630. https://doi.org/10.1016/0092-8674(89)90584-9

Toledo, M., A. Batista-Gonzalez, E. Merheb, M.L. Aoun, E. Tarabra, D. Feng, J. Sarparanta, P. Merlo, F. Botrè, G.J. Schwartz, et al. 2018. Autophagy Regulates the Liver Clock and Glucose Metabolism by Degrading CRY1. *Cell Metab*. 28:268–281.e4. https://doi.org/10.1016/j.cmet.2018.05.023

Tran, E.J., and S.R. Wente. 2006. Dynamic nuclear pore complexes: life on the edge. *Cell*. 125:1041–1053. https://doi.org/10.1016/j.cell.2006.05.027

Webster, B.M., P. Colombi, J. Jäger, and C.P. Lusk. 2014. Surveillance of nuclear pore complex assembly by ESCRT-III/Vps4. *Cell*. 159:388–401. https://doi.org/10.1016/j.cell.2014.09.012

Winey, M., D. Yarar, T.H. Giddings, Jr., and D.N. Mastronarde. 1997. Nuclear pore complex number and distribution throughout the Saccharomyces cerevisiae cell cycle by three-dimensional reconstruction from electron micrographs of nuclear envelopes. *Mol. Biol. Cell*. 8:2119–2132. https://doi.org/10.1091/mbc.8.11.2119

Yang, Z., and D.J. Klionsky. 2010. Eaten alive: a history of macroautophagy. *Nat. Cell Biol*. 12:814–822. https://doi.org/10.1038/ncb0910-814

Zientara-Rytter, K., and S. Subramani. 2019. Mechanistic Insights into the Role of Atg11 in Selective Autophagy. *J. Mol. Biol*. https://doi.org/10.1016/j.jmb.2019.06.017

JCB

Supplemental material

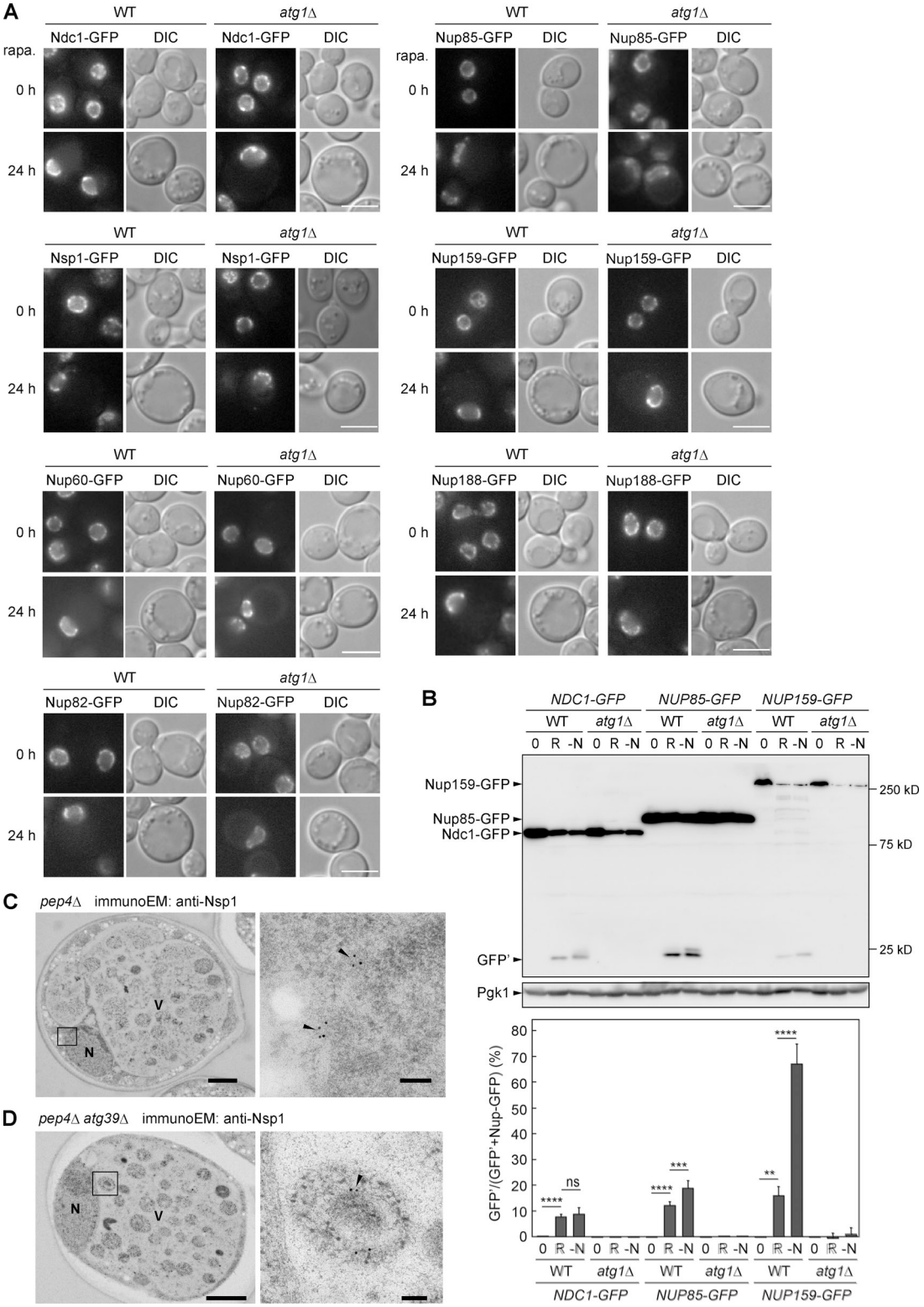

Figure S1. **Nups are degraded by autophagy upon TORC1 inactivation. (A)** Chromosomal Nup genes were fused with the GFP gene, and these cells were observed under a fluorescence microscope. DIC, differential interference contrast microscopy. Scale bars, 5 µm. **(B)** WT and *atg1Δ* cells were treated with rapamycin (R) or incubated in SD-N medium for 24 h, and autophagic degradation of Nup-GFP was examined and measured as described in Fig. 1 B. Error bars represent SD (n = 3). ns, not significant ($P \geq 0.05$); **, $P < 0.01$; ***, $P < 0.001$; ****, $P < 0.0001$ (Tukey's multiple comparisons test). **(C and D)** Immunoelectron microscopy of *pep4Δ* (C) and *pep4Δ atg39Δ* (D) cells was performed as described in Fig. 2 C. The right panels are magnified view of the boxed area in the left panels. Arrowheads show Nsp1 signals (gold particles) in the nuclear envelope (C) or the double-membrane vesicle within the autophagic body (D). Scale bars, 1 µm (left) and 100 nm (right). N, nucleus; V, vacuole.

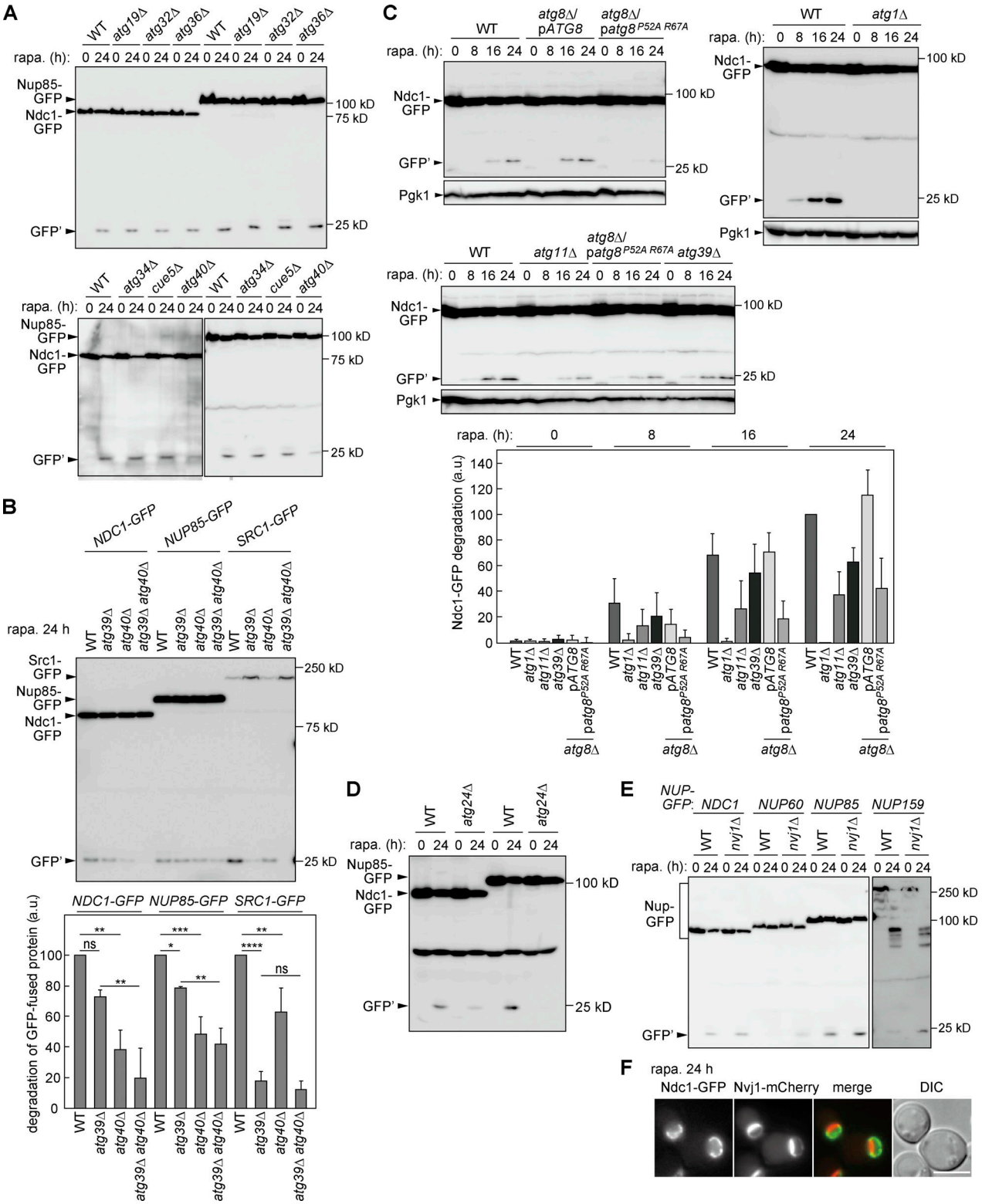

Figure S2. **Degradation of Nups in autophagy-related mutants. (A)** Yeast cells were examined for autophagic degradation of GFP-tagged Nups as described in Fig. 1 B. **(B)** WT, *atg39Δ*, *atg40Δ*, and *atg39Δ atg40Δ* cells expressing Ndc1-GFP, Nup85-GFP or Src1-GFP were treated with rapamycin for 24 h, and degradation of GFP-fused proteins was examined and quantified as described in Fig. 2 A. Error bars represent SD (n = 3). ns, not significant ($P \geq 0.05$); *, $P < 0.05$; **, $P < 0.01$; ***, $P < 0.001$; ****, $P < 0.0001$ (Tukey's multiple comparisons test). **(C)** Yeast cells expressing Ndc1-GFP and carrying plasmids expressing WT Atg8 or the AIM-binding pocket mutant (P52A R67A) or the empty vector were treated with rapamycin, and autophagic degradation of Ndc1-GFP was analyzed by immunoblotting as described in Fig. 2 A. The values for WT cells treated with rapamycin for 24 h were set to 100. Error bars represent SD (n = 3). **(D and E)** Yeast cells were treated with rapamycin for 24 h, and degradation of GFP-fused Nups was examined as described in Fig. 1 B. **(F)** Cells expressing Ndc1-GFP and Nvj1-mCherry were treated with rapamycin for 24 h and observed under a fluorescence microscope. Scale bar, 5 µm.

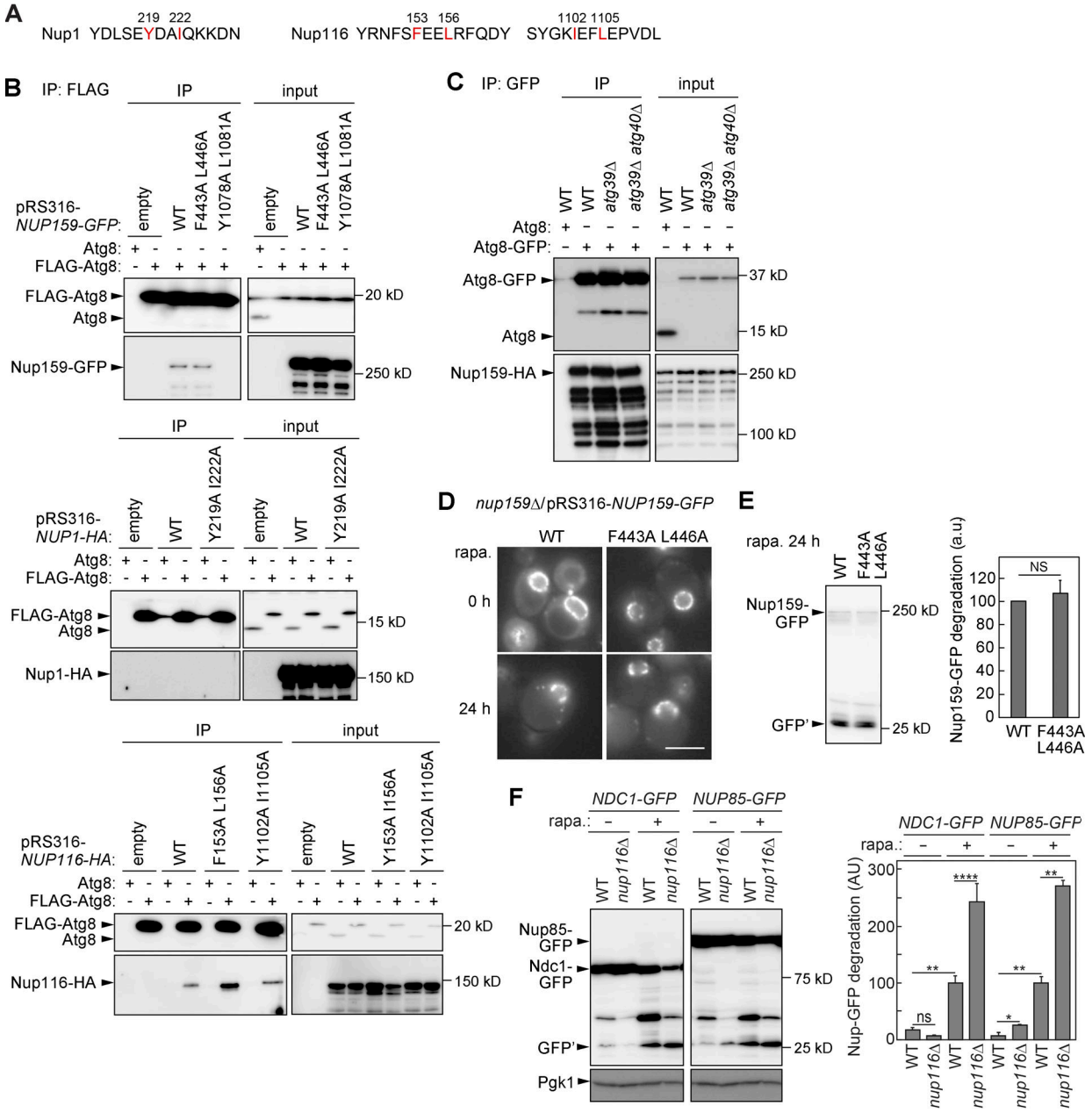

Figure S3. **Analyses of Nup mutants. (A)** The amino acid sequences of the Nup1 and Nup116 regions encompassing putative AIMs predicted in the iLIR database. **(B)** *FLAG-ATG8* cells carrying single-copy plasmids for the expression of Nup159-GFP, Nup116-HA and Nup1-HA were treated with rapamycin for 2 h, followed by coimmunoprecipitation analysis as described in Fig. 3 A. **(C)** WT, *atg39*Δ, and *atg39*Δ *atg40*Δ cells expressing Atg8-GFP and Nup159-HA were subjected to immunoprecipitation as described in Fig. 3 C. **(D)** *nup159*Δ cells carrying *NUP159-GFP* single-copy plasmids were treated with rapamycin for 24 h and observed under a fluorescence microscope. Scale bar, 5 µm. **(E)** The cells used in D were examined for degradation of Nup159-GFP as described in Fig. 2 A. Error bars represent SD (n = 7). NS, not significant (unpaired two-tailed Student's t test). **(F)** WT and *nup116*Δ cells expressing Ndc1-GFP or Nup85-GFP were treated with or without rapamycin for 24 h at 25°C, and degradation of Nup-GFP was examined and measured as described in Fig. 2 A. Error bars represent SD (n = 3). ns, not significant (P ≥ 0.05); *, P < 0.05; **, P < 0.01; ****, P < 0.0001 (Tukey's multiple comparisons test).

Tables S1 and S2 are provided online as separate Excel files. Table S1 shows the results of mass spectrometry of Atg8 immunoprecipitates, and Table S2 lists the yeast strains used in this study.